An explicit/implicit Runge–Kutta-based PFEM model for the simulation of thermally coupled incompressible flows

2 authors:

Julio Marcelo Marti
CIMNE International Center for Numerical Methods in Engineering
30 PUBLICATIONS   **338** CITATIONS

SEE PROFILE

Pavel Ryzhakov
Universitat Politècnica de Catalunya
31 PUBLICATIONS   **290** CITATIONS

SEE PROFILE

Some of the authors of this publication are also working on these related projects:

PEM fuel cell modeling View project

Thermo-mechanical modeling of bottle forming View project

An explicit/implicit Runge-Kutta-based PFEM model for the simulation of thermally coupled incompressible flows

J. Marti[a,b], P.B. Ryzhakov[a]

[a]*Centre Internacional de Mètodes Numèrics en Enginyeria (CIMNE)*
Gran Capitán s/n, 08034 Barcelona, Spain
[b]*Department of Civil and Environmental Engineering, Universitat Politècnica de Catalunya (UPC), 08034 Barcelona, Spain*

Abstract

A semi-explicit Lagrangian scheme for the simulation of thermally coupled incompressible flow problems is presented. The model relies on combining an explicit multi-step solver for the momentum equation with an implicit heat equation solver. Computational cost of the model is reduced via application of an efficient strategy adopted for the solution of momentum/continuity system by the authors in their previous work. The applicability of the method to solving thermo-mechanical problems is studied via various numerical examples.

Keywords: Navier-Stokes, thermo-mechanical, Particle Finite Element Method, Lagrangian, explicit, benchmark, Boussinesq

1. Introduction

Lagrangian finite element models for the simulation of flow problems originated from the ideas presented in [1, 2] and [3]. Unlike their fixed-grid counterparts, Lagrangian fluid models naturally track the evolving boundaries and do not suffer numerical diffusion. Lagrangian fluid approaches have been further developed for free surface flows in [4] and [5] resulting in what is now generally known as the "Particle Finite Element Method" (PFEM), a

---

methodology that combines the features of the classical Lagrangian finite element methods and the mesh-free approaches. The PFEMs have been further advanced by various groups and applied to flows with multi-fluids [6, 7], fluid-structure interactions [8, 9, 10] and multi-fluid-structure interaction problems [11].

Another area where Lagrangian fluid models may be suitable are the thermally coupled flow problems. In such problems PFEMs facilitate convection of the material properties (which, in case of being temperature-dependent, requires solving additional transport equations in case of using fixed grid approaches). This explains why PFEM-based models were successfully used for analyzing polymer melting [12], [13]. PFEM-based models also appear to be suitable for the simulation of material forming processes (e.g. mould filling), also characterized by a strongly coupled thermo-mechanical nature. Since convection is resolved automatically due to Lagrangian nature of the fluid solver, the heat solver in these models involves solely the diffusion (diffusion-radiation) equation [14].

In [15] a Lagrangian-based thermally coupled model was applied to the simulation of metal casting. In [16] a basic strategy for the solution of incompressible fluids with thermal convection and free surfaces using the PFEM was presented. The integration scheme is fully implicit, pressure and velocity are uncoupled via the fractional step approach. Besides, the thermal buoyancy effects are considered by introducing the Boussinesq approximation. This strategy is applied to mould filling in [17]. Similar Lagrangian thermally-coupled approach is used in commercial software $POLYFLOW$ [18] and applied to glass forming simulation in [19]. A PFEM-based model applied to bottle forming can be found in [20, 21].

All the afore-mentioned PFEM-based approaches rely on fully implicit time integration schemes. Unfortunately, this usually results in very high computational costs in case of mesh degradation and thus strongly limits the application of the PFEM-based model to real-life application. As shown in [22] time step restriction cannot be eliminated even by a frequent re-meshing. The possibility of element inversion at any non-linear iteration step leads to an immediate failure of the implicit solver [22]. Thus, all the mentioned approaches require estimating a critical time step in order to ensure that no element gets inverted. In practice, this often introduces a prohibitively small time step restriction. Taking into account that the problem solution at each time step involves non-linear iterations and each non-linear iteration, in turn, requires solving large linear systems, the resulting methods turn out to have

2

a very large computational cost.

In order to alleviate the above-mentioned drawbacks of the iterative procedure involved in an implicit solution, Idelsohn et al [23] proposed a scheme, where particles were moved only once, prior to implicit solution of the Navier-Stokes equations (which was considered linear). Such mesh movement step was fully explicit. The obtained configuration was considered to be the end-of-step configuration and was not further updated. In order to ensure improved accuracy of this prediction, the particle positions were obtained following the streamline corresponding to velocity at the known time step. The advantage of this method was that it allowed using large time steps without falling into the danger of element inversion as the mesh was considered fixed within an implicit step. The methodology that combined fixed background mesh with the moving particles is extended to thermally coupled problems in [24]. There, thermal and viscous diffusivity are treated explicitly. The thermal coupling is carried out via a temperature-dependent buoyancy term added to fluid acceleration (Boussinesq approximation).

An alternative explicit-implicit Lagrangian method was proposed in [25]. There, domain configuration was accurately predicted by using fourth order Runge-Kutta scheme for integrating both the velocity and the particle positions. Due to the implicit nature of the pressure in incompressible flows, pressure was integrated implicitly. The approach introduced re-meshing prior to pressure solution step, ensuring that no element may be inverted during the implicit step. This allowed to alleviate time step restrictions and eliminate its dependence on the mesh deformation. The computational cost of the method was strongly reduced also due to a technique that allowed solving for the pressure only once per time step.

In the present work the explicit-implicit scheme proposed in [25] is extended to thermally coupled problems (a fixed-grid version of the scheme can be consulted in [26] and [27]). For the problems where buoyancy effects are essential, Boussinesq term is added to the fluid acceleration.

The paper is organized as follows: Section 2 presents the governing equations of a thermally coupled incompressible fluid. The solution algorithm is outlined. Section 3 is devoted to solution of various benchmarks. First, a thermal square cavity is solved and the solution is validated using the bibliographic data. Next, a problem involving a thermally coupled fluid flow in a backward facing step is solved. Ultimately, a thermally coupled fluid sloshing example is simulated.

2. Numerical model for thermally coupled incompressible flows

In thermally coupled problems the energy equation is coupled to the momentum/continuity system via the convective velocity. For the low-speed flows with non-negligible buoyancy effects, Boussinesq hypothesis is often employed, provided that temperature gradients are small. It allows to account for the aforementioned thermal buoyancy phenomena using an incompressible flow model [28]. According to this hypothesis the buoyant term of the momentum equation is assumed to be temperature-dependent, while the density is assumed constant everywhere else in the model. Boussinesq solvers allow solving the energy and the momentum-continuity system in a staggered fashion. The popularity of Boussinesq hypothesis is specially related to its practical applicability and the simplicity of its implementation.

In the following the governing equations for a thermally coupled incompressible flow problems are specified and the solution algorithm is presented.

2.1. Governing equations at continuum level

Let $\Omega \subset R^3$ be a bounded domain containing viscous incompressible fluid. We denote the time by t, the Cartesian spatial coordinates by $\mathbf{x} = x_i|_{i=1}^3$, and the vectorial operator of spatial derivatives by $\nabla = \{\partial_{x_i}\}_{i=1}^3$. The evolution of the velocity $\mathbf{v} = \mathbf{v}(\mathbf{x}, t)$, the pressure $p = p(\mathbf{x}, t)$ and the temperature $T = T(\mathbf{x}, t)$ is governed by the following equations:

$$\rho \frac{\partial \mathbf{v}}{\partial t} + \rho(\mathbf{v} \cdot \nabla)\mathbf{v} - \nabla \cdot (\mu \acute{\mathbf{D}}) + \nabla p = \mathbf{f}, \tag{1}$$

$$\nabla \cdot \mathbf{v} = 0, \tag{2}$$

$$\rho C \frac{\partial T}{\partial t} + \rho C \mathbf{v} \cdot \nabla T - \kappa \Delta T = 0. \tag{3}$$

where μ is the fluid dynamic viscosity, ρ is the density, p is the fluid pressure, $\acute{\mathbf{D}} = \frac{1}{2}(\nabla \mathbf{v} + \nabla^T \mathbf{v})$ is the symmetric part of the velocity gradient tensor, C is the heat capacity and κ is the thermal conductivity. According to Boussinesq hypothesis the body force $\mathbf{f}$ is computed as

$$\mathbf{f} = \rho \mathbf{g}[1 - \beta(T - T_0)] \tag{4}$$

where $\mathbf{g}$ is the gravity acceleration, T and T_0 are the actual temperature and the reference temperature, respectively, and β is the thermal diffusion coefficient.

The position $\mathbf{x}$ of a given material particle (which coincides with the mesh node once the problem is discretized) is given by:

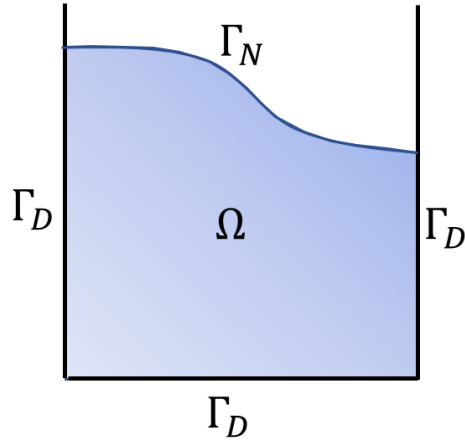$$\frac{D\mathbf{x}}{Dt} = \mathbf{v} \tag{5}$$

Figure 1: Domain and boundaries.

The governing equations are completed with standard Dirichlet and Neumann boundary conditions. On the external boundary $\partial\Omega = \Gamma_D \bigcup \Gamma_N$, such that $\Gamma_D \cap \Gamma_N = \varnothing$. The domain boundaries are shown in Fig. 1.

$$\begin{pmatrix} \mathbf{v} = \bar{\mathbf{v}} \\ T = \bar{T} \end{pmatrix} on \Gamma_D \tag{6}$$

$$\begin{pmatrix} \boldsymbol{\sigma} \cdot \boldsymbol{n} = \overline{\boldsymbol{\sigma}_n} \\ k\boldsymbol{\nabla}T \cdot \boldsymbol{n} = \bar{q}_n \end{pmatrix} on \Gamma_N \tag{7}$$

where $\bar{\mathbf{v}}$ and $\bar{T}$ are the prescribed velocity and temperature respectively, $\mathbf{n}$ is the outer unit normal to Γ_N, $\overline{\boldsymbol{\sigma}_n}$ and $\bar{q}_n$ are the prescribed traction vector and normal heat flux.

The discrete version of the governing equations is presented next.

2.2. Governing equations at discrete level

In the present work, we use a semi-explicit solver of [25] for the mechanical problem and a Backward Euler scheme for the heat equation. An updated Lagrangian reference frame is considered. The semi-explicit solver

5

for the momentum/continuity/position system is based on the fourth-order Runge–Kutta scheme and is characterized by the second order temporal accuracy.

Considering linear finite element approximations for the temperature (note that $\mathbf{N}$ is the vector of shape functions)

$$T\left(\mathbf{x}\right) = \mathbf{N}^T\left(\mathbf{x}\right)\bar{T} \tag{8}$$

heat equation discretized in space and time reads (note absence of the convective term due to adopting the Lagrangian reference frame)

$$\rho C \mathbf{M} \frac{\bar{T}^{n+1}}{\Delta t} + \kappa \mathbf{L}\bar{T}^{n+1} = \rho C \mathbf{M} \frac{\bar{T}^n}{\Delta t}. \tag{9}$$

A linear approximation of the same order is used for the velocity and the pressure

$$p\left(\mathbf{x}\right) = \mathbf{N}^T\left(\mathbf{x}\right)\bar{p} \tag{10}$$

$$\mathrm{v}_i\left(\mathbf{x}\right) = \mathbf{N}^T\left(\mathbf{x}\right)\bar{\mathrm{v}}_i \tag{11}$$

We note that the nodal variables are distinguished from their continuum counterparts by an overbar.

Applying the above spatial approximations and the fourth-order Runge-Kutta time integration scheme, the following equations are obtained (see [25] for further details):

$$\bar{\mathbf{v}}^{n+1} = \bar{\mathbf{v}}^n + \frac{\Delta t}{6}\mathbf{M}^{-1}(\mathbf{r}_1 + 2\mathbf{r}_2 + 2\mathbf{r}_3 + \mathbf{r}_4) - \frac{\Delta t}{6\rho}\mathbf{M}^{-1}\mathbf{G}\bar{p}^{n+1} \tag{12}$$

where intermediate residuals, nodal velocities and positions are defined as:

$$\mathbf{r}_i = \mathbf{G}_{\left(\frac{1}{\rho}\right)}\bar{p}^j - \ \mathbf{K}_{\left(\frac{\mu}{\rho}\right)}\bar{\mathbf{v}}^k + \mathbf{F} \tag{13}$$

$$\bar{\mathbf{v}}^{\beta_i} = \bar{\mathbf{v}}^n + \phi\Delta t\mathbf{M}^{-1}\mathbf{r}_m \tag{14}$$

$$\mathbf{x}^{\beta_i} = \mathbf{x}^n + \gamma\Delta t\bar{\mathbf{v}}^n \tag{15}$$

In the following tables (1-3) i, j, k, m, n, ϕ and γ are summarized for the different variables:

Introducing an intermediate velocity $\tilde{\mathbf{v}}$, following the fractional step approach [29] for decoupling the velocity and the pressure, Eq.(12) can be replaced by the following three equations to be solved sequentially:

$$\tilde{\mathbf{v}} = \bar{\mathbf{v}}^n + \frac{\Delta t}{6}\mathbf{M}^{-1}\left(\mathbf{r}_1 + 2\mathbf{r}_2 + 2\mathbf{r}_3 + \mathbf{r}_4\right) + \frac{\Delta t}{6}\mathbf{M}^{-1}\mathbf{G}_{\left(\frac{1}{\rho}\right)}\bar{p}^n \tag{16}$$

$\mathbf{r}_i$	i	j	k
	1	n	n
	2	n	β_1
	3	β_2	β_2
	4	β_3	β_3

Table 1: Intermediate residuals

$\bar{\mathbf{v}}^{\beta_i}$	i	ϕ	m
	1	1/2	1
	2	1/2	2
	3	1	3

Table 2: Velocities

$\mathbf{x}^{\beta_i}$	i	γ	n
	1	1/2	n
	2	1/2	β_1
	3	1	β_2

Table 3: Nodal positions

$$\frac{\Delta t}{6}\mathbf{L}\bar{p}^{n+1} = \frac{\Delta t}{6}\mathbf{L}\bar{p}^{n} - \mathbf{D}_\rho\tilde{\mathbf{v}} \tag{17}$$

$$\bar{\mathbf{v}}^{n+1} = \tilde{\mathbf{v}} + \frac{\Delta t}{6}\mathbf{M}^{-1}\mathbf{G}_{\left(\frac{1}{\rho}\right)}(\bar{p}^{n+1} - \bar{p}^{n}) \tag{18}$$

Particle's position $\mathbf{x}$ at time $n+1$ can be found as

$$\mathbf{x}^{n+1} = \mathbf{X}^{n} + \frac{\Delta t}{6}(\bar{\mathbf{v}}^{n} + 2\bar{\mathbf{v}}^{\beta 1} + 2\bar{\mathbf{v}}^{\beta 2} + \bar{\mathbf{v}}^{\beta 3}) \tag{19}$$

The matrices in the above equations are defined as:

$$\mathbf{K}_{\left(\frac{\mu}{\rho}\right)} = \sum_{elem}\int_\Omega \frac{\mu}{\rho}\left(\nabla\mathbf{N}^T\nabla\mathbf{N} + \nabla\mathbf{N}^T\nabla^T\mathbf{N}\right)d\Omega \tag{20}$$

$$\mathbf{M} = \sum_{elem}\int_\Omega \mathbf{N}^T\mathbf{N}d\Omega \tag{21}$$

$$\mathbf{F} = \sum_{elem}\int_\Omega \mathbf{N}^T\mathbf{g}d\Omega \tag{22}$$

$$\mathbf{G}_{\left(\frac{1}{\rho}\right)} = \sum_{elem}\int_\Omega \frac{1}{\rho}\nabla\mathbf{N}^T\mathbf{N}d\Omega \tag{23}$$

$$\mathbf{D}_\rho = \sum_{elem}\int_\Omega \rho\mathbf{N}\nabla\mathbf{N}^T d\Omega \tag{24}$$

$$\mathbf{L}_{\left(\frac{1}{\rho}\right)} = \sum_{elem}\int_\Omega \frac{1}{\rho}\nabla\mathbf{N}^T\nabla\mathbf{N}d\Omega \tag{25}$$

Eq.(17) must be stabilized to avoid numerical oscillation due to the equal order of approximation for velocity and pressure. The stabilization technique

used in the present work is the algebraic sub-grid scale method [30]. For the sake of simplicity, stabilization terms are omitted here. They can be consulted in [25] where the mechanical solver was derived.

2.3. Solution algorithm

The problem to be solved can be formulated as: given the nodal positions, the velocity, the pressure and the temperature at time step t^n, find these variables at t^{n+1}. The overall solution strategy according to the method proposed is summarized in Table 4.

1. Knowing the velocity $\mathbf{v}$, pressure p, temperature T and nodal position $\mathbf{x}$ corresponding to time t^n perform the explicit step:
   - For i from 1 to 4
       Evaluate intermediate Runge-Kutta residuals $\mathbf{r}_i$ $(i = 1, ..., 4)$ using Eqs.(13).
       Move particles to the new position $\mathbf{x}$(Eq.(19)).
       Update elemental matrices and vectors according to the new nodal positions (Eqs. 20-25).

2. Re-mesh the fluid domain

3. Perform the implicit step: solve the Poisson's equation for the pressure (Eq.(17)). Result: $\bar{p}^{n+1}$.

4. Correct the velocity to obtain a divergence-free solution. Result: $\bar{\mathbf{v}}^{n+1}$ (Eq.(18)).

5. Solve the heat equation (Eq. (9)). Result: $\bar{T}^{n+1}$

6. Compute the Boussinesq term for the next time step using the obtained temperature (Eq. (4)).

7. Go to the next time step.

Table 4: Lagrangian explicit-implicit solution algorithm for thermally coupled incompressible flow problems.

3. EXAMPLES

The model presented in this paper was implemented by the authors in the open source Kratos Multi-Physics software [31]. In the following, three numerical tests are solved. They validate the thermo-mechanical scheme proposed.

3.1. The thermally driven cavity benchmark

This test models the fluid flow in two-dimensional unitary square. Different temperatures are prescribed and maintained at the vertical walls. Convective transport in this test is known as "natural convection". It develops exclusively due to non-zero temperature gradients. This example is used to test the numerical algorithms designed for the integration of the Navier-Stokes equations in incompressible recirculating flows. Boussinesq approximation [32] is valid due to very small temperature variation.

The input data provided below is taken from the benchmark description given in [33]. The top and the bottom walls are insulated (adiabatic condition is considered) and the velocity at all boundaries is set to zero. Vertical walls' temperatures are T_0=298.5 K (right wall) and T_1=297.5 K (left wall). Fluid inside the cavity is initially at rest. Its initial temperature equals the mean of the temperatures on the vertical walls. The scheme of the example is shown in Fig. 2.

The simulations were executed for a range of Rayleigh number ($Ra = \frac{g\beta H^3 \Delta T}{\alpha\nu}$) values: $Ra = 10^6$, $Ra = 10^5$ and $Ra = 10^4$. Prandtl number ($Pr = \frac{\nu}{\alpha}$) was set to (0.71). Note that g, β, α and ν are the gravity, thermal diffusion coefficient, thermal diffusivity and kinematic viscosity, respectively. A constant temperature difference of ΔT=1 K was applied to the two vertical walls, adjusting the thermal diffusion coefficient β until obtaining the desired Rayleigh number, keeping all the other variables constant. The following values were used for the main variables

$\rho = 1 \; \frac{kg}{m^3}$

$\nu = 0.001 \; \frac{m^2}{s}$

$g_y = \text{-10} \; \frac{m}{s^2}$

$\alpha = 0.001 \; \frac{m^2}{s}$

The simulations were carried out using mesh size h =0.015 m and time step dt =0.0025 s.

To validate the present numerical results, the obtained results are compared for different Ra values with the data found in bibliography [33, 34, 35] and [36, 24]. The values and the locations of maximum horizontal and vertical velocities are considered. The comparison is summarized in Tables 5-7.A nearly exact match in terms of the maximum vertical and horizontal velocity for the entire range of the considered Rayleigh numbers is observed. For $Ra = 10^6$ and $Ra = 10^4$ the results are compared against the fixed grid simulations of [33], [36] and the combined PFEM-Eulerian simulation of [24]. For $Ra = 10^5$ no results are presented in [36] and [24], thus the comparison is made only with [33]. One can see a very good agreement among the results. Largest discrepancy is observed in the location of the maximum vertical velocity. One can see that for $Ra = 10^6$ the difference between the compared values is as high as 20 %. For smaller Rayleigh number this discrepancy diminishes.

Results shown in Fig. 3 compare the isotherms obtained in our simulations with those corresponding to the reference solution [37]. The results are in very good agreement with the benchmark solution.

Fig. 4 shows the horizontal velocity profiles in the cavity along the vertical line at x=0.5. One can see that the present results coincide with those of [36] for all the considered values of Rayleigh number.

The results of the present method are compared against those of the former version of thermally coupled purely Lagrangian implicit PFEM model in Fig. 5. Rayleigh number considered here is $Ra = 10^6$ and nine isotherms are shown so as to facilitate the comparison with the reference results. Fig. 5 a) shows the solution obtained in the present work, while Fig. 5 b) and c) display the isotherms of the reference solution [33] and the PFEM model of [38], respectively. One can see that all the isotherms in the upper part of the graphs are nearly identical for all the models, while the third isotherm (counted from the bottom) obtained by the present approach exhibits a much closer match to the reference solution than the former PFEM model, where the isotherm is considerably shifted towards the bottom.

3.2. Heat transfer for backward facing step duct flows

This example models the well-known backward facing step duct flow, which is one of the very commonly simulated CFD problems. Although the geometry of the test is simple, it is characterized by complex flow physics.
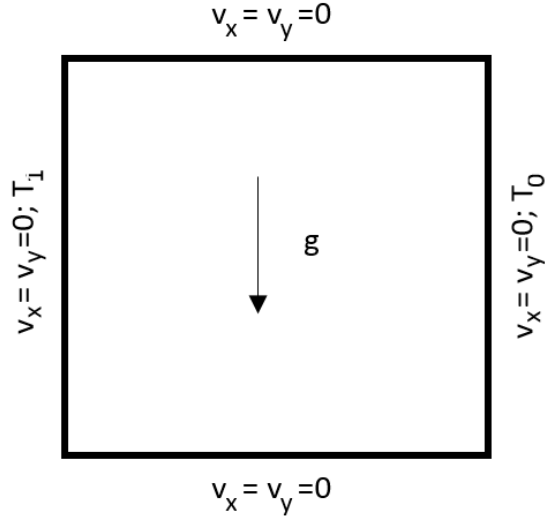
Figure 2: Boundary conditions for thermal cavity benchmark problem

Ra	Data	RK	Davis [33]	Corzo [36]	Sklar [24]
10^6	$v_{x,max}(x=0.5)$	65.45	65.81	64.558	64.483
10^6	y_{max}	0.85	0.852	0.851	0.845
10^6	$v_{y,max}(y=0.5)$	213.07	214.64	221.572	218.054
10^6	x_{max}	0.0474	0.0396	0.067	0.037

Table 5: Numerical solution for the thermal square cavity, Ra=10^6. Comparison with [33], [36], [24].

Ra	Data	RK	Davis
10^5	$v_{x,max}(x=0.5)$	34.924	34.870
10^5	y_{max}	0.862	0.855
10^5	$v_{y,max}(y=0.5)$	67.910	67.910
10^5	x_{max}	0.0576	0.067

Table 6: Numerical solution for the thermal square cavity, Ra=10^5. Comparison with [33].

This example is commonly used to validate conjugate heat transfer models [39]. In our case for the sake of simplicity heat transfer is modeled only in a single homogeneous fluid.

Geometrical details, boundary and initial conditions of the problem are depicted in Fig. 6. The problem was simulated for two values of Reynolds
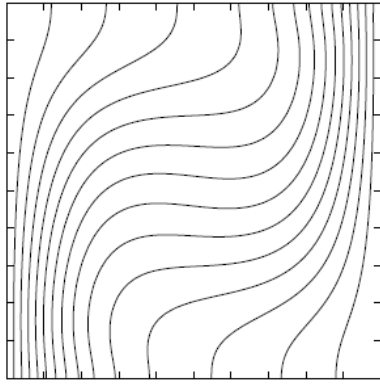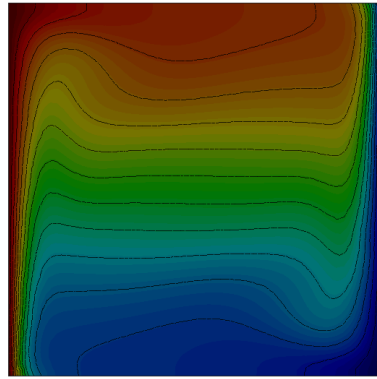
(a) Ra=10^4, [37]
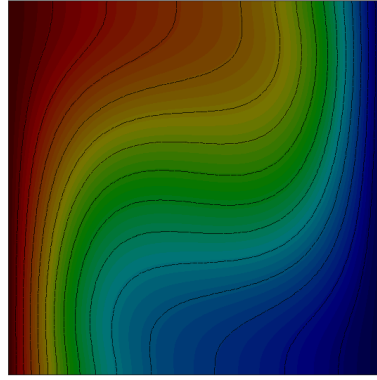
(b) Ra=10^4, RK
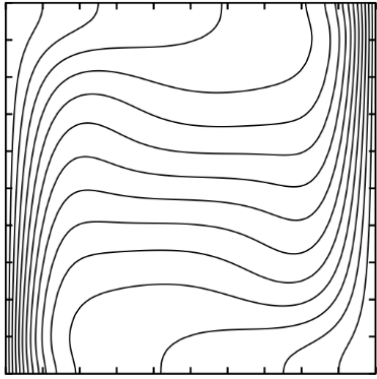
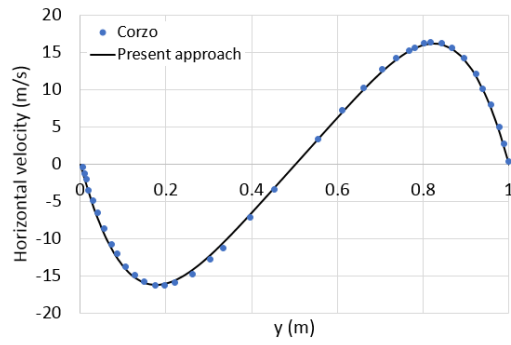(c) Ra=10^5, [37]
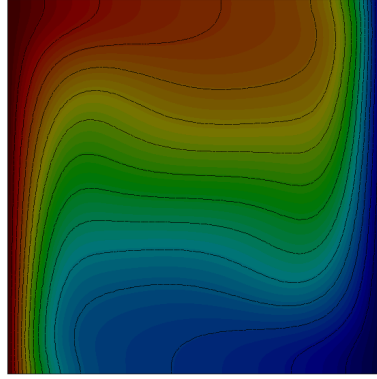
(d) Ra=10^5, RK
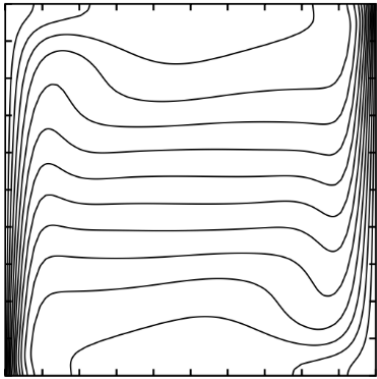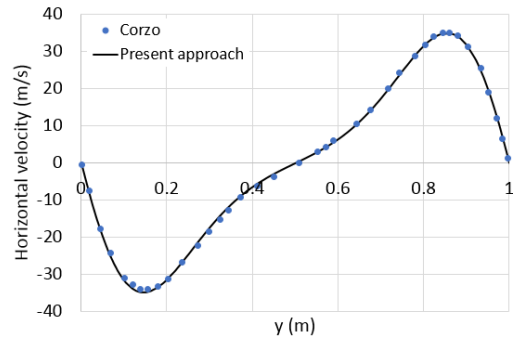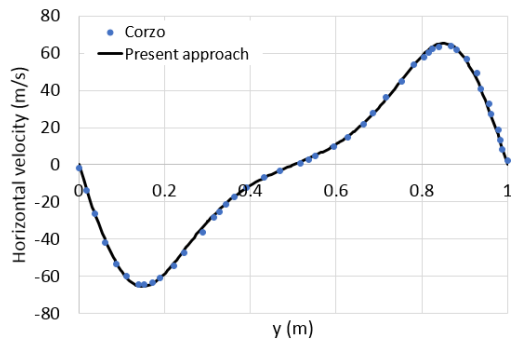
(e) Ra=10^6, [37]

(f) Ra=10^6, RK

Figure 3: Natural convection in a square cavity. Temperature field and iso-lines. Comparison with [37]. Blue and red colors in the present method results (RK) correspond to 297.5 and 298.5 K, respectively.

12

(a) Ra=10^4

(b) Ra=10^5

(c) Ra=10^6

Figure 4: Natural convection in a square cavity. Horizontal velocity profiles along the vertical cut at x=0.5. Comparison with [36]

13

Ra	Data	RK	Davis [33]	Corzo [36]	Sklar [24]
10^4	$v_{x,max}(x=0.5)$	16.250	16.182	16.282	15.982
10^4	y_{max}	0.821	0.823	0.822	0.824
10^4	$v_{y,max}(y=0.5)$	19.541	19.509	19.547	19.378
10^4	x_{max}	0.115	0.120	0.123	0.116

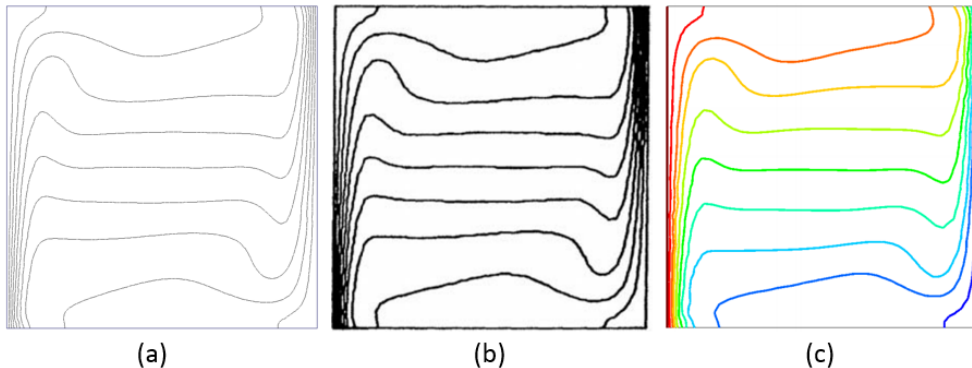Table 7: Numerical solution for the thermal square cavity, Ra=10^4. Comparison with [33], [36], [24].

Figure 5: Natural convection in a square cavity, isotherms. a) present work b) [33] c) [38].

number: Re=100 and Re=800. Prandtl number was maintained identical in both cases: Pr= 0.71. Fluid conductivity was set as κ =0.02 $W/(m \cdot K)$. Gravity is neglected.

Obtained velocity and temperature fields are shown in Figs. 7 - 10. The results obtained using the present semi-explicit model are compared with those of an implicit fixed-grid model. The latter solver was validated and applied to the thermally coupled backward facing step in [40].

The correlation between the solutions obtained for Re=100 using the present model and the Eulerian model can be seen in Fig. 7 (velocity) and Fig. 8 (temperature). The solutions are nearly identical.

For Re=800 some differences between the Lagrangian and the Eulerian simulation results manifest. As can be seen from in Figs. 9 and 10 the cold fluid entering from the left reattaches on the solid wall at approximately x=6 m. After the reattachment point, the cold fluid in contact with the relatively hot solid wall is heated. A hot spot that appears in the fluid region extending from x=0 to the reattachment point results from the fluid trapped
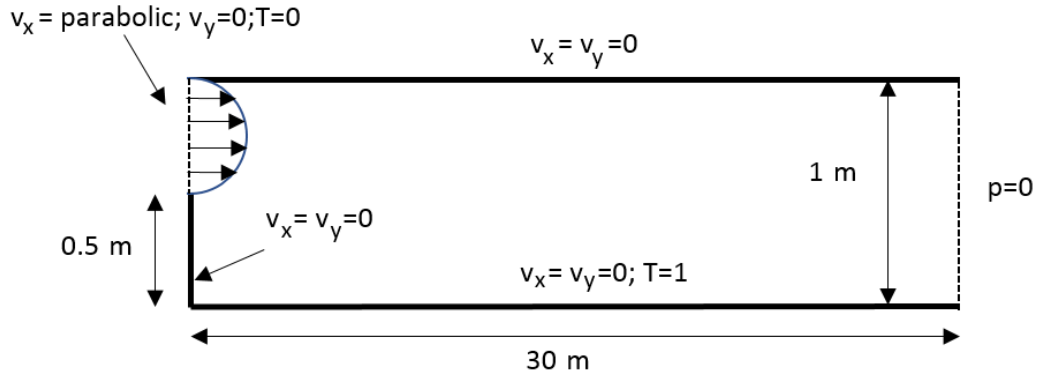
Figure 6: Thermally coupled backward facing step. Geometric details, initial and boundary conditions.

between the entering fluid stream and the channel. However, the posterior development of the thermal boundary layer downstream of the impingement point is slightly different. This is related with the evolution of the velocity that can be observed in detail in Fig. 12 which affects the evolution of the heated layer of fluid. While the Eulerian model exhibits a steady-state solution, the Lagrangian model shows a periodic solution. The difference is particularly evident in the vicinity of the step. Nevertheless, the velocity and the temperature distributions are very similar in the entire domain. This issue requires further investigation as the same periodic behavior was obtained when applying fomerly proposed implicit schemes as well.

Temperature profiles along the vertical axis recorded at x=6, 14 and 30 are plotted in Figs.11 and 12. Once again, one can see that for Re=100 Eulerian and Lagrangian solutions are coincident. For Re=800 present approach slightly deviates from the reference solution due to the unsteady nature of the flow in the vicinity of the step. This difference is largest along the horizontal axis of the channel at y=0.5. Further away from the step the solutions completely coincide.
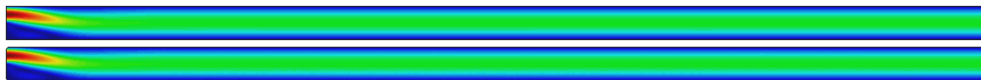

Figure 7: Thermally coupled backward facing step. Velocity magnitude contours (Re=100, Pr=0.71) at 40 sec. Eulerian (above) vs Lagrangian (below) simulation results. Red and blue colors stand for 1.5 and 0 m/s, respectively.
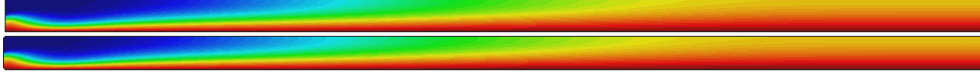
15

Figure 8: Thermally coupled backward facing step. Temperature contours (Re=100, Pr=0.71) at 40 sec. Eulerian (above) vs Lagrangian (below) simulation results. Red and blue colors stand for 0 and 1 C, respectively.
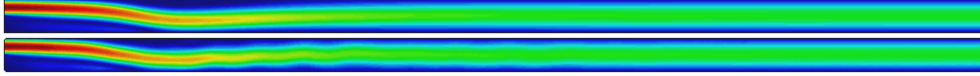

Figure 9: Thermally coupled backward facing step. Velocity magnitude contours (Re=800, Pr=0.71) at 40 sec. Eulerian (above) vs Lagrangian (below) simulation results. Red and blue colors stand for 1.5 and 0 m/s, respectively.
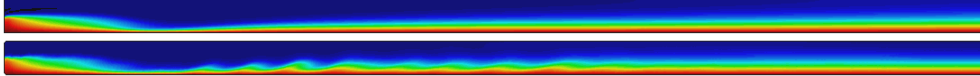

Figure 10: Thermally coupled backward facing step. Temperature contours (Re=800, Pr=0.71) at 40 sec. Eulerian (above) vs Lagrangian (below) simulation results. Red and blue colors stand for 0 and 1 C, respectively.

3.3. Sloshing in a hot container

While previous examples involved analysis of problems with fixed boundaries and were solved for the sake of the solver validation, next test deals with a problem that involves a domain with moving boundaries. It deals with a free-surface flow in a container with hot walls. Tests of this kind were proposed in [41] for illustrating the capability of thermally coupled PFEM-solvers. The example focuses on the impact of temperature-induced viscosity changes upon the flow behavior.

Domain configuration at t=0 is shown in Fig. 13. No-slip boundary condition is prescribed at all the walls of the domain. Free surface (zero tractions) condition is prescribed at the free surface. The dimensions of the domain are: H=0.1 m and h=0.02 m. The free surface shape is sinusoidal. The properties are: density $\rho = 1000$ kg/m^3, gravity $g = -9.8$ m/s^2.

Initial temperature of the fluid is set to $T_0 = 273$ K. Walls are kept at a fixed temperature: T_w (the simulation is carried out for three values of wall temperature: 273, 373 and 473 K). The viscosity is computed from the temperature using the following expression:
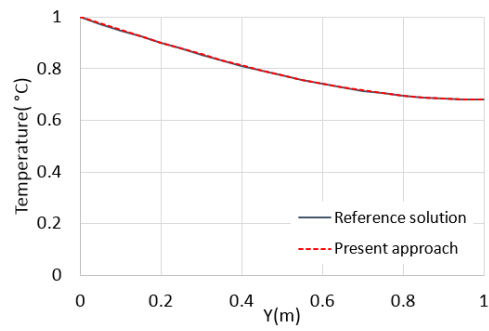
$$\nu = -2.996 \cdot T^3 \cdot 10^{-7} + 0.000379 \cdot T^2 - 0.161 \cdot T + 23.12 \qquad (26)$$

16

(a) x=6.
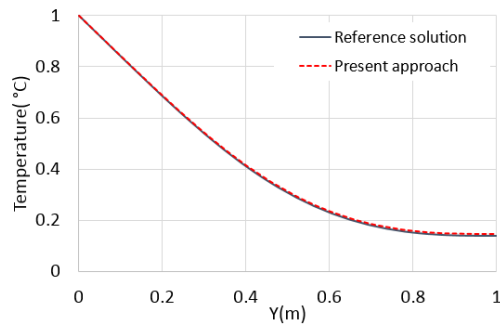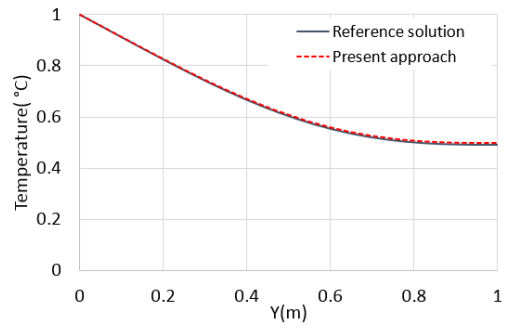
(b) x=14.

(c) x=30.

Figure 11: Thermally coupled backward facing step. Comparison of temperature profiles at x=6; 14 and 30 for the case of Re=100. Eulerian (reference) [40] vs Lagrangian (present approach) simulation results.

(a) x=6.
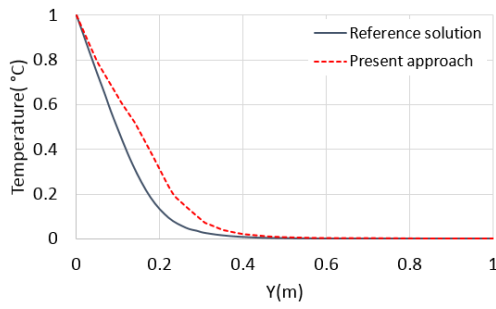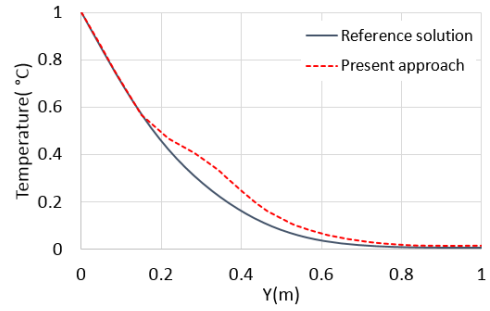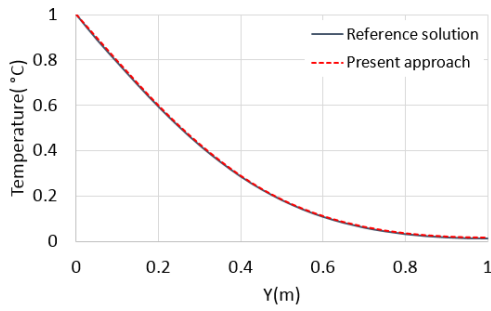

(b) x=14.

(c) x=30.

Figure 12: Thermally coupled backward facing step. Comparison of temperature profiles at x=6; 14 and 30 for the case of Re=800.

(a) Initial domain geometry
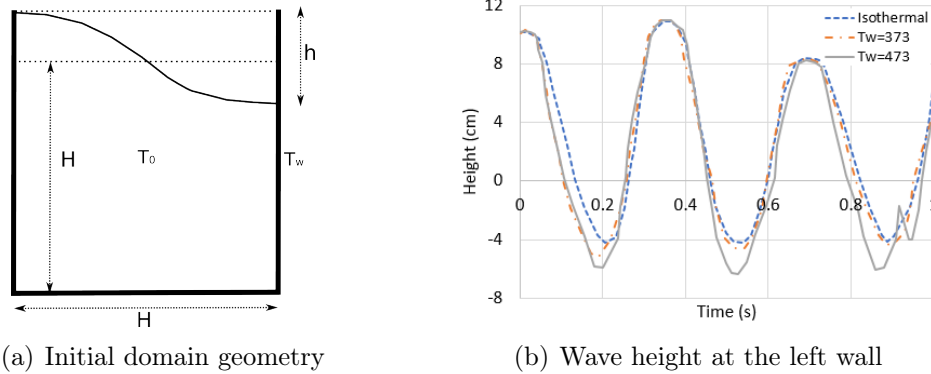

(b) Wave height at the left wall

Figure 13: Free-surface fluid sloshing in a hot container.

The above formula mimics the relative viscosity change of water between 273 and 473 K [42]. The heat capacity C and the conductivity κ of the fluid were set to: 4000.0 $J/(kg \cdot K)$ and 2000.0 $W/(m \cdot K)$, respectively.

A total time of 1 s is simulated. The domain is discretized with an unstructured triangular mesh of size 0.002 m (6000 elements approximately).

We test the impact of the thermal effects upon the fluid behavior considering that the walls of the container are hot. Domain configurations showing temperature distributions are shown at various time instances in Fig. 14. As the temperature propagates (mainly due to diffusion in the present case) from the walls into the fluid volume, the viscosity changes and the differences in the free surface location becomes more and more evident. In particular, at t=0.9 s the case characterized by the highest wall temperature exhibits a significantly different solution, as the temperature increases significantly nearly in the entire domain (except for the small area in the center). Attaining lower viscosity the fluid moves faster, therefore, e.g. at 0.9 s the crest of the wave moves further from the right wall as the temperature of the walls growth.

The example above shows that for the free-surface flow problems characterized by temperature changes, the present fluid solver may be advantageous as it allows to easily account for temperature-dependent viscosity by simply adding a diffusion solver to an efficient semi-explicit mechanical solver.

(a) $T_w = 273$ K, t=0.2 s (b) $T_w = 273$ K, t=0.4 s (c) $T_w = 273$ K, t=0.9 s

(d) $T_w = 373$ K, t=0.2 s (e) $T_w = 373$ K, t=0.4 s (f) $T_w = 373$ K, t=0.9 s

(g) $T_w = 473$ K, t=0.2 s (h) $T_w = 473$ K, t=0.4 s (i) $T_w = 473$ K, t=0.9 s
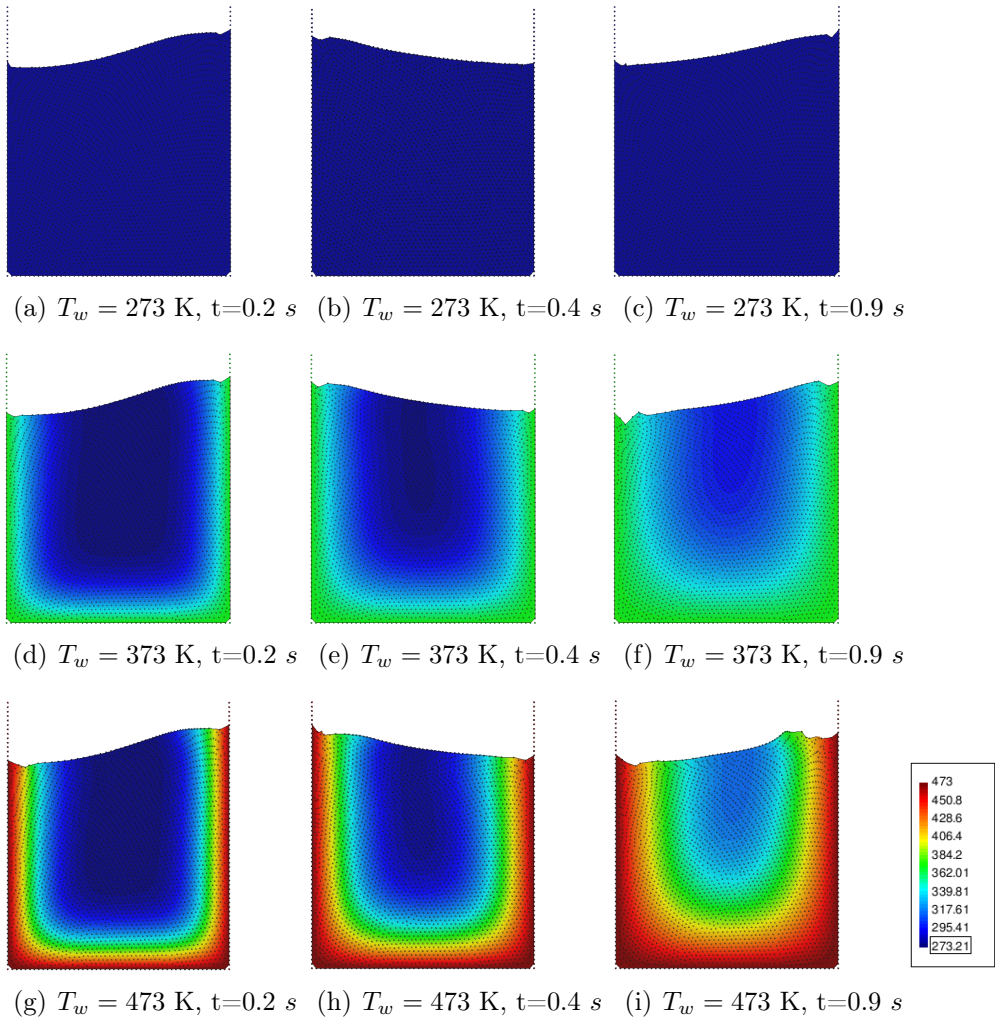
Figure 14: Sloshing in a hot container. Temperature distribution at various time instances.

4. Summary and conclusion

In this paper a semi-explicit incompressible flow model was coupled to a heat equation solver. Being fully Lagrangian, the model automatically resolves convection and the heat module solves only the transient diffusion equation. The model belongs to the second generation of the Particle Finite Element Method solvers, where the particles-nodes are moved explicitly prior to the solution of the implicit problem. The solver for the thermally coupled flows presented here inherits the advantages of the mechanical solver formerly proposed by the authors in [25], namely the possibility of using constant time step.

The thermal coupling was validated using several benchmark cases. The validation tests revealed that the proposed solver provides reliable solutions. Being semi-explicit the solver provides an attractive alternative to the fully implicit models, provided that the time step estimates are favorable. In particular, since in the mechanical part of the solver only the pressure is treated implicitly, favorable time step can be encountered in problems characterized by low viscosity values. For the flows characterized by high viscosity, the proposed solver is not advantageous (e.g. the casting problems, or melting problems where material viscosity at low temperatures is typically very high). This occurs due to the time step size restriction introduced by the explicit treatment of the viscous term. However, it is beneficial for thermo-mechanical fluid flow problems characterized by temperature-dependent viscosity.

Conflict of interests. On behalf of all authors, the corresponding author states that there is no conflict of interest.

[1] B. Ramaswamy, M. Kawahara, and T. Nakayama. Lagrangian finite element method for the analysis of two-dimensional sloshing problems. International Journal for Numerical Methods in Fluids, 6(9):659–670, 1986.

[2] B. Ramaswamy and M. Kawahara. Lagrangian finite element analysis applied to viscous free surface fluid flow. International Journal for Numerical Methods in Fluids, 7(9):953–984, 1987.

[3] R. Radovitzky and M. Ortiz. Lagrangian finite element analysis of Newtonian fluid flows. International Journal for Numerical Methods in Engineering, 43(4):607–619, 1998.

[4] E. Oñate, S.R. Idelsohn, F. Del Pin, and A. Romain. The particle finite element method: an overview. International Journal of Computational Methods, 1(02):267–307, 2004.

[5] S.R Idelsohn, E. Oñate, and F. Del Pin. The particle finite element method: a powerful tool to solve incompressible flows with free-surfaces and breaking waves. International Journal of Numerical Methods in Engineering, 61:964–989, 2004.

[6] S.R. Idelsohn, M. Mier-Torrecilla, and E. Oñate. Multi-fluid flows with the particle finite element method. Computer methods in applied mechanics and engineering, 198(33-36):2750–2767, 2009.

[7] S.R. Idelsohn, M. de Mier-Torrecilla, J. Marti, and E. Oñate. The particle finite element method for multi-fluid flows. In Particle-Based Methods, pages 135–158. Springer, 2011.

[8] S.R Idelsohn, J. Marti, A. Limache, and E. Oñate. Unified Lagrangian formulation for elastic solids and incompressible fluids. Application to fluid-structure interaction problems via the PFEM. Computer Methods in Applied Mechanics and Engineering, 197:1762–1776, 2008.

[9] M. Zhu and M. H. Scott. Unified fractional step method for Lagrangian analysis of quasi-incompressible fluid and nonlinear structure interaction using the PFEM. International Journal for Numerical Methods in Engineering, 109(9):1219–1236, 2017.

[10] P.B. Ryzhakov. A modified fractional step method for fluid–structure interaction problems. Revista Internacional de Métodos Numéricos para Cálculo y Diseño en Ingeniería, 33(1-2):58–64, 2017.

[11] P.B. Ryzhakov and E. Oñate. A finite element model for fluid–structure interaction problems involving closed membranes, internal and external fluids. Computer Methods in Applied Mechanics and Engineering, 326:422–445, 2017.

[12] E. Oñate, J. Marti, P.B. Ryzhakov, R. Rossi, and S.R. Idelsohn. Analysis of the melting, burning and flame spread of polymers with the particle finite element method. Computer Assisted Methods in Engineering and Science, 20(3):165–184, 2017.

[13] J. Marti, S.R. Idelsohn, and E. Oñate. A finite element model for the simulation of the ul-94 burning test. Fire Technology, 54(6):1783–1805, 2018.

[14] J. Marti, P.B Ryzhakov, S.R. Idelsohn, and E. Oñate. Combined Eulerian–PFEM approach for analysis of polymers in fire situations. Int. J. Numer. Meth. Engng., 92:782–801, 2010.

[15] F. Muttin, T. Coupez, M. Bellet, and J.-L. Chenot. Lagrangian finite-element analysis of time-dependent viscous free-surface flow using an automatic remeshing technique: Application to metal casting flow. International Journal for Numerical Methods in Engineering, 36(12):2001–2015, 1993.

[16] R. Aubry, S.R. Idelsohn, and E. Oñate. Particle finite element method in fluid-mechanics including thermal convection-diffusion. Computers and Structures, 83(17):1459 – 1475, 2005. Advances in Meshfree Methods.

[17] E. Oñate, J. Rojek, M. Chiumenti, S.R. Idelsohn, F. Del Pin, and R. Aubry. Advances in stabilized finite element and particle methods for bulk forming processes. Computer methods in applied mechanics and engineering, 195(48-49):6750–6777, 2006.

[18] ANSYS polyflow. https://www.ansys.com/products/fluids/ansys-polyflow. Accessed: 2018-12-20.

[19] M. Hyre. Numerical simulation of glass forming and conditioning. Journal of the American Ceramic Society, 85(5):1047–1056, 2002.

[20] P.B. Ryzhakov, J. Garcia, and E. Oñate. Lagrangian finite element model for the 3D simulation of glass forming processes. Computers & Structures, 177:126–140, 2016.

[21] P. B. Ryzhakov. An axisymmetric PFEM formulation for bottle forming simulation. Computational Particle Mechanics, 4(1):3–12, 2017.

[22] P.B. Ryzhakov, J. Marti, S.R. Idelsohn, and E. Oñate. Fast fluid–structure interaction simulations using a displacement-based finite element model equipped with an explicit streamline integration prediction. Computer Methods in Applied Mechanics and Engineering, 315:1080–1097, 2017.

[23] S.R. Idelsohn, J. Marti, P. Becker, and E. Oñate. Analysis of multifluid flows with large time steps using the particle finite element method. International Journal for Numerical Methods in Fluids, 75(9):621–644, 2014.

[24] D.M. Sklar, J.M. Gimenez, N.M. Nigro, and S.R. Idelsohn. Thermal coupling in particle finite element method-second generation. Mecánica Computacional, 31:4143–4152, 2012.

[25] J. Marti and P.B. Ryzhakov. An explicit-implicit finite element model for the numerical solution of incompressible Navier-Stokes equations on moving grids. submitted to: Computer Methods in Applied Mechanics and Engineering.

[26] P.B. Ryzhakov and J. Marti. A semi-explicit multi-step method for solving incompressible Navier-Stokes equations. Applied Sciences, 8(1):119, 2018.

[27] P.B. Ryzhakov, R. Rossi, and E. Oñate. An algorithm for the simulation of thermally coupled low speed flow problems. International Journal for Numerical Methods in Fluids, 70(1):1–19, 9 2012.

[28] D.A. Nikulin. Applicability of the boussinesq approximation for the solution of problems of unsteady natural concentration convection. Fluid Dynamics, 17(5):779–781, 1982.

[29] Chorin A.J. A numerical method for solving incompressible viscous problems. Journal of Computational Physics, 2:12–26, 1967.

[30] R. Codina. A stabilized finite element method for generalized stationary incompressible flows. Computer Methods in Applied Mechanics and Engineering, 190(20-21):2681 – 2706, 2001.

[31] P. Dadvand, R. Rossi, and E. Oñate. An object-oriented environment for developing finite element codes for multi-disciplinary applications. Archieves of Computational Methods in Engineering, 17/3:253–297, 2010.

[32] V.S. Arpaci and P.S. Larsen. Convection Heat Transfer. Prentice Hall, New York, 1984.

[33] G.D.V Davis. Natural convection of air in a square cavity: a benchmark numerical solution. International Journal for Numerical Methods in Fluids, 3:249–264, 1983.

[34] R.J.A. et al. Janssen. Transition to time-periodicity of a natural-convection flow in 3D differentially heated cavity. Int.J.Heat Mass Transfer, 36:2927–2940, 1993.

[35] A. Friki. Simulation numerique 3D, en collocation Chebyshev, de phenomenes thermoconvectifs en centrifugation. These de l'Universite Paris-Sud XI- Orsay, 1993.

[36] S. Corzo, S. Márquez, D. Ramajo, and N. Nigro. Numerical simulation of natural convection phenomena. ENIEF, Rosario, Argentina, 2011.

[37] H.N. Dixit and V. Babu. Simulation of high Rayleigh number natural convection in a square cavity using the lattice Boltzmann method. International Journal of Heat and Mass Transfer, 49(3):727 – 739, 2006.

[38] M. Mier Torrecilla. Numerical simulation of multi-fluid flows with the Particle Finite Element Method. Ph. D. thesis,Universitat Politècnica de Catalunya, 2010.

[39] M. Ramsak. Conjugate heat transfer of backward-facing step flow: A benchmark problem revisited. International Journal of Heat and Mass Transfer, 84:791 – 799, 2015.

[40] J. Marti. Exploration of kratos thermo-fluid capabilities for conjugate heat transfer problems. Technical report, CIMNE, 2018.

[41] A. Franci. Unified lagrangian formulation for fluid and solid mechanics, fluid-structure interaction and coupled thermal problems using the PFEM. Springer, isbn 978-3319833415, 2016.

[42] Engineering toolbox. https://www.engineeringtoolbox.com/water-dynamic-kinematic-viscosity-d_596.html. Accessed: 2018-12-20.